APL Materials

Non-local architecture for spin current manipulation in silicon platforms

Cite as: APL Mater. 11, 021102 (2023); https://doi.org/10.1063/5.0130759
Submitted: 14 October 2022 • Accepted: 11 January 2023 • Published Online: 01 February 2023

C. Zucchetti, F. Scali, P. Grassi, et al.

© 2023 Author(s).

Non-local architecture for spin current manipulation in silicon platforms

Cite as: APL Mater. 11, 021102 (2023); doi: 10.1063/5.0130759
Submitted: 14 October 2022 • Accepted: 11 January 2023 •
Published Online: 2 February 2023

View Online
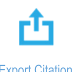
Export Citation

CrossMark

C. Zucchetti, F. Scali, P. Grassi, M. Bollani, L. Anzi, G. Isella, M. Finazzi, F. Ciccacci, and F. Bottegoni[a)]

AFFILIATIONS

Dipartimento di Fisica, Politecnico di Milano, Piazza Leonardo da Vinci 32, 20133 Milano, Italy

[a)]Author to whom correspondence should be addressed: federico.bottegoni@polimi.it

ABSTRACT

We have developed a non-local architecture for spin current injection, manipulation, and detection in *n*-doped bulk Si at room temperature. Spins are locally generated at the indirect gap of bulk Si by means of circularly polarized light and then detected by exploiting the inverse spin-Hall effect (ISHE) occurring inside a thin Pt pad deposited at the top of the Si substrate. We demonstrate that it is possible to modulate the transport properties of the optically injected spin current by applying a bias voltage along the direction of motion of the particles. In this case, we are able to explore both the spin diffusion regime, characterized by a spin diffusion length $L_s \approx 12\ \mu$m, and the spin drift regime with applied electric fields up to $E = 35$ V/cm. We demonstrate that the spin transport length of the electrons can be increased (or decreased) by more than 100% for electric fields antiparallel (or parallel) to the diffusion direction. As a consequence, the ISHE signal can be electrically controlled to have high or low output voltages from the non-local device.

© 2023 Author(s). All article content, except where otherwise noted, is licensed under a Creative Commons Attribution (CC BY) license (http://creativecommons.org/licenses/by/4.0/). https://doi.org/10.1063/5.0130759

The integration of novel spin-based devices in CMOS-compatible platforms is one of the great challenges of modern spintronics. To this aim, it would be highly desirable to design spintronic architectures in bulk silicon substrates.[1–3] This would further add functionalities provided by the spin degree of freedom to the palette of digital/analogic operations of common electronic devices, improving the performances of integrated circuits without revolutionizing the industrial supply chain.

In this context, Si-based heterostructures have gained momentum as platforms for spintronic applications in the past years,[4] thanks to the advances in engineering efficient non-local architectures,[5] mainly four-terminal devices, for electrical spin generation and detection in a wide range of temperatures and doping concentrations.[1,2,6] Electrical spin injection by means of magnetic tunnel junctions has been efficiently achieved in heavily *n*-doped Si at low[7] and room temperature,[8–10] whereas spin-polarized hot electron injection[11] has been successfully employed at low temperatures in lightly *n*-doped or undoped Si to circumvent the conductivity mismatch.[12] Finally, optical spin injection has proven to be an alternative route for spin injection in Si,[13–15] since it allows generating a spin-oriented population of electrons at the Si indirect gap ($E_{ig} = 1.12$ eV at $T = 300$ K). A spin polarization of a few percent can be reached at room temperature as a consequence of phonon-mediated optical transitions.[16,17]

At variance with spin injection, spin manipulation in Si still remains an unsolved task, mainly due to the low spin–orbit interaction, which fosters spin transport, allowing for spin lifetimes of the order of 10 ns at room temperature,[1,13,15] but results in low electrically driven effective magnetic fields,[14,18,19] preventing spin precession by means of voltage gates.[1,2] Indeed, seminal reports indicate that the electrical manipulation of spins could be achieved only in Si-based quantum wells or thin films, at least at low temperatures.[2,20] Therefore, literature reports have focused on the large spin diffusion length, suggesting that Si could be employed for spin interconnects,[6] thanks to its good spin injection and detection efficiency,[1,2,6–10] but relegating possible spin-based logic operations to high-*Z* or magnetic thin films,[21] eventually grown on top of Si. However, technological applications of spin-based devices require the electrical control of the output signals, which could be performed by manipulating the spin current rather than directly the spin.

In this respect, we propose a non-local architecture for spin current injection, manipulation, and detection in lightly *n*-doped bulk

© Author(s) 2023

Si at room temperature. We exploit optical orientation to inject a spin current at the indirect gap of bulk Si, and we detect the inverse spin-Hall effect[22] (ISHE) signal generated in a thin Pt pad grown on top of the Si substrate. We show that the ISHE signal can be modulated by applying a bias voltage along the direction of motion of the spin-polarized electrons. We characterize the spin transport in the Si platform in both the spin diffusion and the spin drift regime with applied electric fields up to $E = 35$ V/cm, where the spin transport length of the electrons can be increased (decreased) by more than 100% for electric fields antiparallel (parallel) to the diffusion direction.

The investigated sample is shown in Fig. 1(a). A set of 8 nm-thick and 40×3 μm^2-wide Pt pads, used as spin injectors, has been deposited by e-beam evaporation on top of a lightly phosphorous-doped Si(001) substrate (donor concentration $N_d \approx 1 \times 10^{15}$ cm^{-3}), previously etched to obtain a 1.8 μm-thick and 300×50 μm^2-wide mesa. The center-to-center distance between the two consecutive pads is 6 μm. Referring to the sample scheme of Fig. 1(a), the first Pt pad on the left is employed as a spin detector; therefore, it is slightly larger than the other pads (8 nm-thick and 40×5 μm^2-wide) and is contacted with two Au/Ti electrodes. The latter are obtained by electron beam evaporation of 7 nm of Ti, 70 nm of Au, 7 nm of Ti, and 100 nm of Al followed by lift-off. These contacts allow detecting the voltage drop ΔV under open-circuit conditions, generated at the two edges of the spin detector due to the ISHE taking place within the Pt pad.[22] A 150 nm-thick SiO_2 layer [shown in green in Fig. 1(a)] has been deposited between the Si substrate and the Au/Ti contacts to avoid direct spin and charge absorption from the semiconductor to the electrodes. Finally, two Al/Au/Ti ohmic contacts have been deposited at the ends of the Si mesa along the x axis of the sample

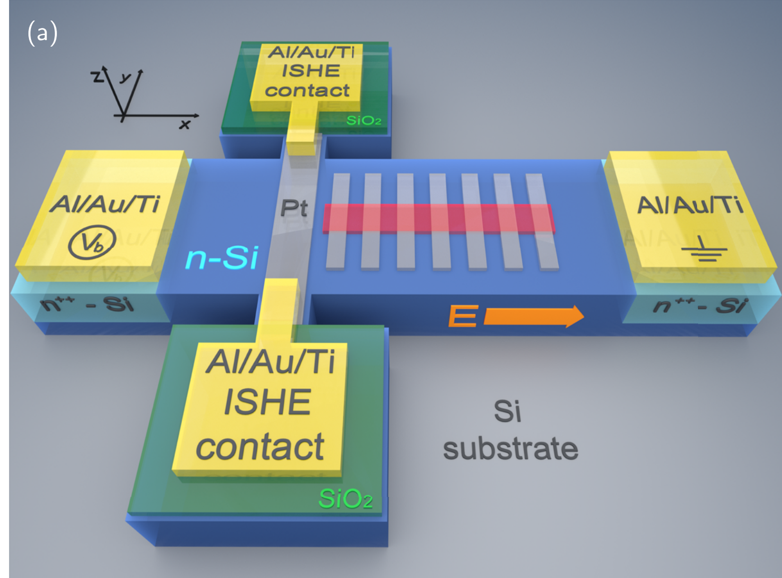

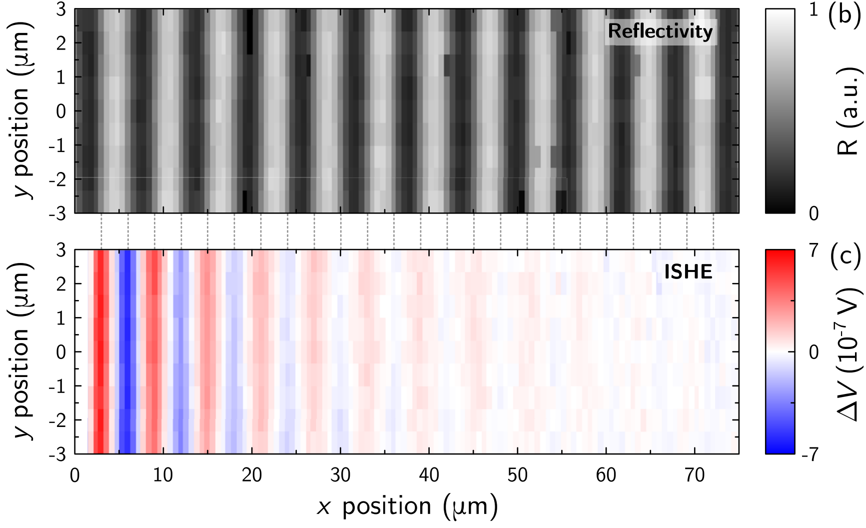

FIG. 1. (a) Sample structure and experimental geometry for non-local optical spin orientation and ISHE detection measurements (not to scale). A series of Pt pads is grown on top of a Si mesa to inject the spin-polarized electrons at different distances with respect to the ISHE detector (first Pt pad on the left). The latter is contacted by means of two Au/Ti contacts. Two Al/Au/Ti ohmic contacts are deposited at the end of the Si mesa. By applying a bias voltage $V_b \neq 0$ between these contacts, one can generate an electric field along the x axis of the sample. Reflectivity (b) and ISHE (c) map for $h\nu = 1.5$ eV, $W_i = 7$ μW with no applied bias, acquired within the red region of panel (a). The origin of the x axis is set at correspondence with the position of the right edge of the Pt detector.

© Author(s) 2023

to apply the bias voltage V_b. The suppression of the Schottky barrier at the Ti/Si interface has been obtained by heavily doping the region beneath the ohmic contacts by means of the spin-on-dopant (SOD) technique.[23,24]

All the measurements have been performed at room temperature by exploiting a confocal microscopy setup (see Refs. 15, 25, and 26), in which the sample surface is scanned by a laser beam. The circular polarization of the light is modulated at 50 kHz by means of a photoelastic modulator (PEM), and the incident light is focused on the sample by an objective with 0.7 numerical aperture, obtaining a diffraction-limited spot size on the sample of the order of the light wavelength. The reflectivity (R) and ISHE (ΔV) signals have been simultaneously recorded by a photodetector and a lock-in amplifier, respectively.

Optical spin injection is performed by illuminating the Pt pads with the circularly polarized laser beam. At correspondence with opposite edges of each pad, the phase and the amplitude of the incident electromagnetic field are modulated so that phonon-mediated optical transitions generate two symmetric spin populations at the indirect gap of Si,[13,17] with opposite spin projections along the x axis.[15,25–28] The presence of several Pt pads enables us to locally inject spins at different distances from the spin detector.

Spin-polarized carriers then diffuse toward the Pt detector, possibly driven by the electric field along x and enter the first Pt pad on the left [see Fig. 1(a)] by means of thermionic emission,[13,29] overcoming the Schottky barrier formed at the interface between Pt and Si.[30] Inside Pt, the inverse spin-Hall effect takes place through spin-dependent scattering with Pt nuclei. This spin-to-charge conversion produces a voltage drop ΔV at the edges of the ISHE detector. Since the spin current flows along the z axis inside Pt and ΔV is measured along y, only the x component of the spin polarization vector can be detected.[15,22,31] The latter is generated in the optical orientation process, thanks to the Pt pads, whose exploitation as spin injectors allows matching the requirements imposed by the ISHE process.[27]

For the sake of clarity, it is worth bearing in mind that the optical orientation process in Si generates spin-polarized electrons at the Δ valleys and spin-polarized holes at Γ. However, the literature suggests that the hole spin lifetime lies in the picosecond range,[8,32] whereas the electron spin lifetime is of the order of tens of nanoseconds [see Fig. 3(c)].[13,33,34] Therefore, as a first approximation, we can suppose that the ISHE signal is mainly produced by spin-polarized electrons, neglecting the hole contribution.[13]

Figures 1(b) and 1(c) show the reflectivity (R) and the ISHE (ΔV) map acquired in a $75 \times 6\ \mu m^2$-wide region of the sample, represented by the red window in Fig. 1(a). A pigtailed laser diode with photon energy $h\nu = 1.5$ eV and incident power $W_i = 7\ \mu$W has been employed as the optical source. The origin of the x axis is set at correspondence with the position of the right edge of the Pt detector. ΔV changes sign when the light beam illuminates opposite edges of each Pt pad due to the opposite projection of the spin polarization vector along x and exponentially decreases when the distance between the injection and detection point is increased. This is further highlighted in Figs. 2(a) and 2(b), which show the profiles of R and ΔV, respectively, obtained by integrating the signal along y within the investigated sample region.

The amplitude of the ISHE signal as a function of the x position, evaluated at correspondence with the left edge of each Pt injector,

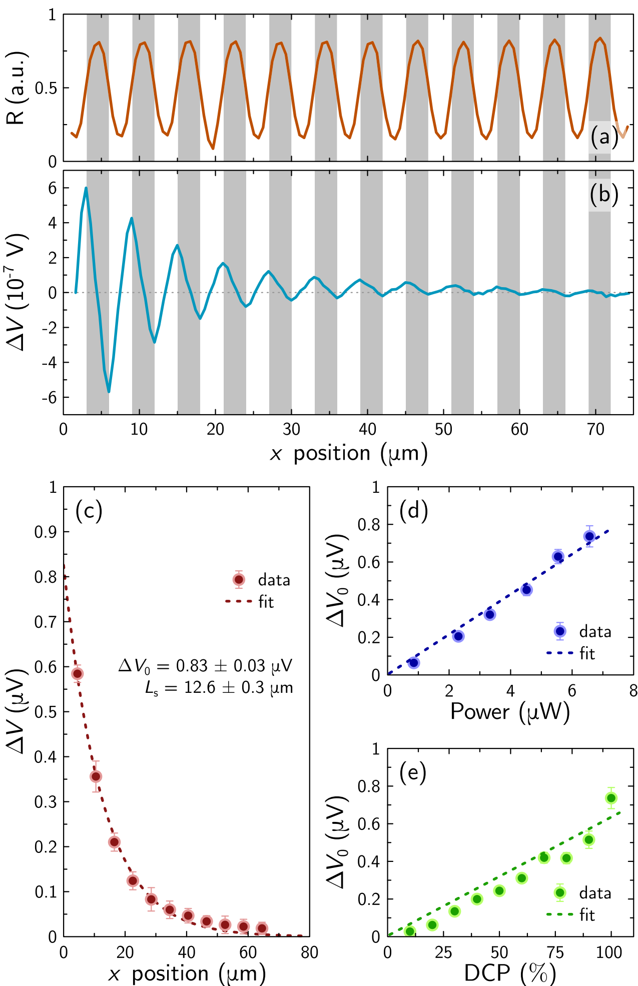

FIG. 2. Reflectivity R (a) and ISHE signal ΔV (b) profiles, obtained by integrating the signal of Figs. 1(b) and 1(c) along y, respectively. (c) ISHE signal ΔV (red dots) as a function of the distance from the Pt detector, evaluated at correspondence with the left edge of each Pt injector. The dashed red line represents the fit of the experimental data by means of the function of Eq. (1), resulting from a one-dimensional spin diffusion model with no applied bias. ΔV dependence on (d) the incident optical power W_i and (e) the degree of circular polarization (DCP).

can be exploited to estimate the electron spin diffusion length L_s with no applied bias, as shown in Fig. 2(c). Indeed, the experimental data can be fitted with the one-dimensional spin diffusion model,[35]

$$\Delta V = \Delta V_0 e^{-x/L_s}, \tag{1}$$

obtaining $L_s = 12.6 \pm 0.3\ \mu$m, which yields an electron spin lifetime $\tau_s = L_s^2/D_e \approx 40$ ns, with $D_e = 36\ cm^2/s$ being the electron diffusion coefficient for lightly doped Si.[36] Such a value is in agreement with previous literature reports, where τ_s in Si have been estimated with different experimental techniques.[1,2,13,15,30]

Furthermore, we have characterized the ISHE signal by acquiring different ΔV maps as a function of the incident power W_i

© Author(s) 2023

and of the degree of circular polarization (DCP) of the light. For each map, a ΔV profile has been obtained and then fitted with the one-dimensional spin diffusion model of Eq. (1), to estimate the dependence of ΔV_0 upon DCP and W_i, as shown in Figs. 2(d) and 2(e), respectively. As expected, ΔV is proportional to DCP and W_i;[15,31,37] therefore, these datasets confirm the spin-related nature of the detected signal.

We have then performed optical spin injection as a function of the incident photon energy, by exploiting a supercontinuum laser,[38] delivering photons in the 0.6–2 eV energy range. In this case, spin-polarized electrons are promoted in the conduction band along the Δ direction with a different kinetic energy, which definitely affects the electron spin diffusion length [see Fig. 3(a)] and, as a consequence, the electron spin lifetime τ_s, as shown in Fig. 3(b). Each L_s value has been obtained by fitting the corresponding ΔV profile at fixed $h\nu$ with Eq. (1). For $h\nu \approx E_{ig}$ and $L_s \approx 70$ μm, L_s drastically decreases with increasing $h\nu$. The origin of such a behavior stems from the fact that for $h\nu \approx E_{ig}$, the spin-polarized electrons are promoted at the bottom of the conduction band at the Δ valleys and spin relaxation is mainly driven by spin-dependent scattering with impurity centers.[39] Since the Si substrate is only lightly doped, the spin lifetime is quite large. On the contrary, when $h\nu$ is increased, spin-polarized electrons are promoted in the Si conduction band with an energy larger than the indirect energy gap and spin relaxation mainly occurs via spin-dependent scattering with phonons.[33,34] In this respect, we have calculated the photon energy dependence of τ_s [green solid line in Fig. 3(b)], by taking into account the spin–flip cross sections within the Yafet–Elliot picture[40,41] for phonon-driven inter-$\Delta\Delta$ and intravalley scattering as well as for spin-dependent scattering with impurities.[39] The deformation potentials and the energies of the phonon branches in Si, involved in the spin-relaxation processes, have been taken from Ref. 42. The calculation is in fairly good agreement with the experimental results and other literature reports,[33,34] although our model overestimates τ_s for $h\nu \to E_{ig}$. Such a discrepancy could be explained considering that in Ref. 43, the intervalley spin–flip mechanism in Si has been mostly ascribed to the spin-dependent scattering with impurity centers rather than with phonons, whereas in our calculation, the former is only considered as an intravalley process. Although the spin-relaxation channel proposed in Ref. 43 should become relevant only for heavily doped Si, it could still determine the slight difference between the experimental and calculated values of τ_s in the low photon-energy range.

Finally, we have investigated the bias dependence of the ISHE signal by applying a voltage difference between the ohmic contacts at the two sides of the Si mesa sketched in Fig. 1(a). In this case, an electric field E_x is applied along the x axis of the sample, which corresponds to the direction of motion of the spin-polarized electrons. Positive and negative V_b values are applied to the left ohmic contact of the sample [see Fig. 1(a)], whereas the right one is always grounded. The experimental results are shown in Fig. 4(a), where the ΔV profiles for $h\nu = 1.5$ eV and $W_i = 7$ μW as a function of the x position are compared for different values of the bias voltage V_b, comprised between ±7.5 V. For $V_b > 0$, the decay length of the ISHE signal, in this case also named *spin transport length* $L_{s,t}$, is evidently increased, since the spin-polarized electrons are accelerated by the applied electric field E_x toward the Pt detector. On the contrary, for $V_b < 0$, the spin-polarized electrons are slowed down by the presence of E_x, and therefore, $L_{s,t}$ is strongly quenched. A quantitative analysis on the experimental data can be performed by fitting the ΔV profiles of Fig. 4(a) with the one-dimensional model of Eq. (1), provided that the spin diffusion length L_s is replaced with $L_{s,t}$, to take into account the spin drift regime of the spin-polarized electrons.[26] Figure 4(b) shows the dependence of $L_{s,t}$ upon the electric field E_x in the investigated V_b range. The former has been estimated from V_b by means of numerical simulations considering the three-dimensional field distribution in the sample. For $V_b = 0$, $L_{s,t}$ approximately matches the L_s value obtained above, since for $V_b = 0$, the spin diffusion regime is restored. However, for $V_b = 7.5$ V, i.e., $E_x = 35$ V/cm, $L_{s,t}$ is enhanced by more than 100%, where $L_{s,t} \approx 30$ μm. On the contrary, if $V_b < 0$, the spin transport length is suppressed down to $L_{s,t} \approx 3$ μm for $V_b = -7.5$ V ($E_x = -35$ V/cm).

The bias dependence of $L_{s,t}$, evaluated from the experimental data of Fig. 4(a), can also be compared to the spin transport length calculated from the analytical solution of the one-dimensional coupled spin continuity and spin drift-diffusion equations [solid green line in Fig. 4(b)],[26,44–47]

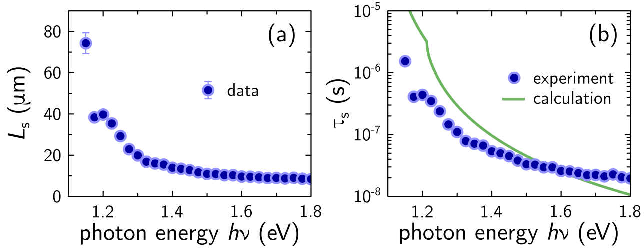

FIG. 3. (a) Photon energy dependence of the electron spin diffusion length L_s. (b) Photon energy dependence of the electron spin lifetime τ_s (blue dots), evaluated by considering experimental data of panel (a) and the electron diffusion coefficient $D_e = 36$ cm^2/s. The green solid line represents the calculated dependence of τ_s upon $h\nu$, by taking into account spin-relaxation cross sections with impurities and phonons for spin-polarized electrons at the Si indirect gap.

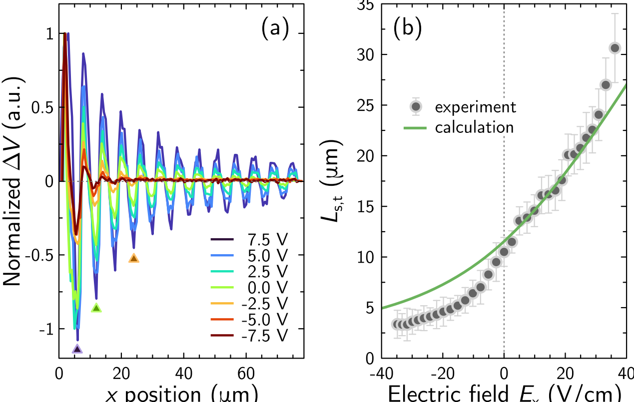

FIG. 4. (a) ΔV profiles as a function of the x position for bias voltages -7.5 V < V_b < 7.5 V. (b) Experimental (gray dots) and calculated (green solid line) dependence of the spin transport length $L_{s,t}$ upon the applied electric field E_x.

© Author(s) 2023

$$L_{s,t} = \left[-\frac{eE_x}{2k_B T} + \sqrt{\left(\frac{eE_x}{2k_B T}\right)^2 + \frac{1}{L_s^2}} \right]^{-1}, \quad (2)$$

with k_B being the Boltzmann constant, e being the elementary charge, and T being the lattice temperature. Equation (2) reproduces the experimental trend of $L_{s,t}$ and is able to capture all the essential parameters involved in the spin current modulation. The latter are basically a *finite* spin diffusion length L_s, comparable to the device length, and an applied electric field $|E_x| < 2k_B T/(eL_s)$. We have also performed two-dimensional (2D) finite-element spin-transport simulations on the xz plane, and we have found that the agreement with the experimental results is not significantly improved.[26] Anyway, the experimental data of Fig. 4(b) indicate that the electrical spin current manipulation can be efficiently achieved in bulk Si at room temperature. A closer inspection of the ISHE signal at a fixed distance with respect to the Pt detector reveals that the proposed non-local architecture basically acts as a spintronic logic gate. Indeed, if the spin current is injected at distances from the Pt detector larger than L_s [for example, $x = 2L_s$, see Fig. 5(a)], it is possible to observe a complete electrical modulation of ΔV between $V_b = -2.5$ V and $V_b = 2.5$ V, which represents a voltage range fully compatible with those already exploited in integrated circuits. In this case, the two bias-dependent outputs of the device (ΔV) can be exploited as logic signals. On the contrary, if spins are generated at distances from the ISHE detector comparable or lower than L_s, it is mandatory to increase the voltage range to detect a full signal modulation [for $x = L_s$, $V_b = \pm 5$ V, see Fig. 5(b)]. Eventually, no significant ΔV modulation is observed in the investigated bias range at $x = L_s/2$ [see Fig. 5(c)]. It is worth noticing that L_s can be properly reduced by increasing the doping concentration of the semiconductor,[48] in order to match the typical dimensions of common electronic devices.

In conclusion, we have demonstrated a non-local architecture for spin injection, transport, and detection in lightly n-doped bulk Si. By exploiting thin Pt pads deposited on top of the Si substrate, it is possible to locally inject a spin current with a projection of the spin polarization in the plane of the device, which can then be detected by means of ISHE in a Pt detector. We have shown that the spin current can be completely modulated by applying an electric field along the direction of motion of the spin-polarized electrons, in order to obtain a high or low signal output, depending on the direction of the applied electric field. These results pave the way to the design and engineering of a novel class of spintronic devices, based on spin-dependent logic operations.

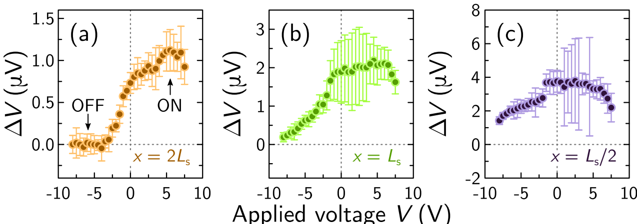

FIG. 5. ISHE signal as a function of V_b for optical spin injection at a fixed distance x from the Pt detector equal to (a) $x = 2L_s$, (b) $x = L_s$, and (c) $x = L_s/2$.

AUTHOR DECLARATIONS

Conflict of Interest

The authors have no conflicts to disclose.

Author Contributions

C. Zucchetti: Conceptualization (equal); Data curation (equal); Formal analysis (equal); Investigation (equal); Methodology (equal); Software (equal); Supervision (equal); Validation (equal); Visualization (equal). **F. Scali**: Data curation (equal); Investigation (equal); Software (equal). **P. Grassi**: Data curation (equal); Investigation (equal). **M. Bollani**: Data curation (equal); Formal analysis (equal); Investigation (equal); Methodology (equal). **L. Anzi**: Data curation (equal); Investigation (equal); Methodology (equal). **G. Isella**: Formal analysis (equal); Methodology (equal). **M. Finazzi**: Conceptualization (equal); Formal analysis (equal); Supervision (equal); Validation (equal). **F. Ciccacci**: Conceptualization (equal); Supervision (equal); Validation (equal). **F. Bottegoni**: Conceptualization (equal); Data curation (equal); Investigation (equal); Methodology (equal); Supervision (equal); Validation (equal); Writing – original draft (equal).

DATA AVAILABILITY

The data that support the findings of this study are available from the corresponding author upon reasonable request.

REFERENCES

[1] R. Jansen, "Silicon spintronics," Nat. Mater. **11**, 400–408 (2012).
[2] V. Sverdlov and S. Selberherr, "Silicon spintronics: Progress and challenges," Phys. Rep. **585**, 1–40 (2015).
[3] E. Talamas Simola, V. Kiyek, A. Ballabio, V. Schlykow, J. Frigerio, C. Zucchetti, A. De Iacovo, L. Colace, Y. Yamamoto, G. Capellini, D. Grützmacher, D. Buca, and G. Isella, "CMOS-compatible bias-tunable dual-band detector based on GeSn/Ge/Si coupled photodiodes," ACS Photonics **8**, 2166–2173 (2021).
[4] A. Ferrari, F. Bottegoni, G. Isella, S. Cecchi, and F. Ciccacci, "Epitaxial $Si_{1-x}Ge_x$ alloys studied by spin-polarized photoemission," Phys. Rev. B **88**, 115209 (2013).
[5] F. Rortais, C. Vergnaud, A. Marty, L. Vila, J.-P. Attané, J. Widiez, C. Zucchetti, F. Bottegoni, H. Jaffrès, J.-M. George, and M. Jamet, "Non-local electrical spin injection and detection in germanium at room temperature," Appl. Phys. Lett. **111**, 182401 (2017).
[6] H. Dery, Y. Song, P. Li, and I. Žutić, "Silicon spin communication," Appl. Phys. Lett. **99**, 082502 (2011).
[7] O. M. J. van't Erve, A. T. Hanbicki, M. Holub, C. H. Li, C. Awo-Affouda, P. E. Thompson, and B. T. Jonker, "Electrical injection and detection of spin-polarized carriers in silicon in a lateral transport geometry," Appl. Phys. Lett. **91**, 212109 (2007).
[8] S. P. Dash, S. Sharma, R. S. Patel, M. P. de Jong, and R. Jansen, "Electrical creation of spin polarization in silicon at room temperature," Nature **462**, 491–494 (2009).
[9] K.-R. Jeon, B.-C. Min, I.-J. Shin, C.-Y. Park, H.-S. Lee, Y.-H. Jo, and S.-C. Shin, "Electrical spin accumulation with improved bias voltage dependence in a crystalline CoFe/MgO/Si system," Appl. Phys. Lett. **98**, 262102 (2011).
[10] A. Spiesser, H. Saito, Y. Fujita, S. Yamada, K. Hamaya, S. Yuasa, and R. Jansen, "Giant spin accumulation in silicon nonlocal spin-transport devices," Phys. Rev. Appl. **8**, 064023 (2017).
[11] I. Appelbaum, B. Huang, and D. J. Monsma, "Electronic measurement and control of spin transport in silicon," Nature **447**, 295–298 (2007).

© Author(s) 2023

[12]B.-C. Min, K. Motohashi, C. Lodder, and R. Jansen, "Tunable spin-tunnel contacts to silicon using low-work-function ferromagnets," Nat. Mater. **5**, 817–822 (2006).
[13]F. Bottegoni, C. Zucchetti, F. Ciccacci, M. Finazzi, and G. Isella, "Optical generation of pure spin currents at the indirect gap of bulk Si," Appl. Phys. Lett. **110**, 042403 (2017).
[14]C. Zucchetti, F. Bottegoni, G. Isella, M. Finazzi, F. Rortais, C. Vergnaud, J. Widiez, M. Jamet, and F. Ciccacci, "Spin-to-charge conversion for hot photoexcited electrons in germanium," Phys. Rev. B **97**, 125203 (2018).
[15]F. Bottegoni, C. Zucchetti, G. Isella, M. Bollani, M. Finazzi, and F. Ciccacci, "Spin–charge interconversion in heterostructures based on group-IV semiconductors," LA Riv. Nuovo Cimento **43**, 45–96 (2020).
[16]P. Li and H. Dery, "Theory of spin-dependent phonon-assisted optical transitions in silicon," Phys. Rev. Lett. **105**, 037204 (2010).
[17]J. L. Cheng, J. Rioux, J. Fabian, and J. E. Sipe, "Theory of optical spin orientation in silicon," Phys. Rev. B **83**, 165211 (2011).
[18]F. Bottegoni, A. Calloni, G. Bussetti, A. Camera, C. Zucchetti, M. Finazzi, L. Duò, and F. Ciccacci, "Spin polarized surface resonance bands in single layer Bi on Ge(111)," J. Phys.: Condens. Matter **28**, 195001 (2016).
[19]T. Guillet, A. Marty, C. Vergnaud, M. Jamet, C. Zucchetti, G. Isella, Q. Barbedienne, H. Jaffrès, N. Reyren, J.-M. George, and A. Fert, "Large Rashba unidirectional magnetoresistance in the Fe/Ge(111) interface states," Phys. Rev. B **103**, 064411 (2021).
[20]R. Jansen, B.-C. Min, and S. P. Dash, "Oscillatory spin-polarized tunnelling from silicon quantum wells controlled by electric field," Nat. Mater. **9**, 133–138 (2010).
[21]A. Manchon, J. Železný, I. M. Miron, T. Jungwirth, J. Sinova, A. Thiaville, K. Garello, and P. Gambardella, "Current-induced spin–orbit torques in ferromagnetic and antiferromagnetic systems," Rev. Mod. Phys. **91**, 035004 (2019).
[22]E. Saitoh, M. Ueda, H. Miyajima, and G. Tatara, "Conversion of spin current into charge current at room temperature: Inverse spin-Hall effect," Appl. Phys. Lett. **88**, 182509 (2006).
[23]M. Bollani, M. Salvalaglio, A. Benali, M. Bouabdellaoui, M. Naffouti, M. Lodari, S. D. Corato, A. Fedorov, A. Voigt, I. Fraj, L. Favre, J. B. Claude, D. Grosso, G. Nicotra, A. Mio, A. Ronda, I. Berbezier, and M. Abbarchi, "Templated dewetting of single-crystal sub-millimeter-long nanowires and on-chip silicon circuits," Nat. Commun. **10**, 5632 (2019).
[24]C. Barri, E. Mafakheri, L. Fagiani, G. Tavani, A. Barzaghi, D. Chrastina, A. Fedorov, J. Frigerio, M. Lodari, F. Scotognella, E. Arduca, M. Abbarchi, M. Perego, and M. Bollani, "Engineering of the spin on dopant process on silicon on insulator substrate," Nanotechnology **32**, 025303 (2021).
[25]C. Zucchetti, F. Bottegoni, C. Vergnaud, F. Ciccacci, G. Isella, L. Ghirardini, M. Celebrano, F. Rortais, A. Ferrari, A. Marty, M. Finazzi, and M. Jamet, "Imaging spin diffusion in germanium at room temperature," Phys. Rev. B **96**, 014403 (2017).
[26]C. Zucchetti, A. Marchionni, M. Bollani, F. Ciccacci, M. Finazzi, and F. Bottegoni, "Electric field modulation of spin transport," APL Mater. **10**, 011102 (2022).
[27]F. Bottegoni, M. Celebrano, M. Bollani, P. Biagioni, G. Isella, F. Ciccacci, and M. Finazzi, "Spin voltage generation through optical excitation of complementary spin populations," Nat. Mater. **13**, 790–795 (2014).
[28]T. Guillet, C. Zucchetti, A. Marchionni, A. Hallal, P. Biagioni, C. Vergnaud, A. Marty, H. Okuno, A. Masseboeuf, M. Finazzi, F. Ciccacci, M. Chshiev, F. Bottegoni, and M. Jamet, "Spin orbitronics at a topological insulator–semiconductor interface," Phys. Rev. B **101**, 184406 (2020).
[29]C. Zucchetti, G. Isella, F. Ciccacci, M. Finazzi, and F. Bottegoni, "Spin transport and spin-charge interconversion phenomena in Ge-based structures," in *Spintronics XII*, edited by H.-J. M. Drouhin, J.-E. Wegrowe, and M. Razeghi (SPIE, 2019), Vol. 1109033, p. 111.
[30]F. Bottegoni, C. Zucchetti, G. Isella, E. Pinotti, M. Finazzi, and F. Ciccacci, "Modeling the photo-induced inverse spin-Hall effect in Pt/semiconductor junctions," J. Appl. Phys. **124**, 033902 (2018).
[31]K. Ando, M. Morikawa, T. Trypiniotis, Y. Fujikawa, C. H. W. Barnes, and E. Saitoh, "Photoinduced inverse spin-Hall effect: Conversion of light-polarization information into electric voltage," Appl. Phys. Lett. **96**, 082502 (2010).
[32]E. Shikoh, K. Ando, K. Kubo, E. Saitoh, T. Shinjo, and M. Shiraishi, "Spin-pump-induced spin transport in p-type Si at room temperature," Phys. Rev. Lett. **110**, 127201 (2013).
[33]J. L. Cheng, M. W. Wu, and J. Fabian, "Theory of the spin relaxation of conduction electrons in silicon," Phys. Rev. Lett. **104**, 016601 (2010).
[34]Y. Song and H. Dery, "Analysis of phonon-induced spin relaxation processes in silicon," Phys. Rev. B **86**, 085201 (2012).
[35]J. Fabian, A. Matos-Abiague, C. Ertler, P. Stano, and I. Žutić, "Semiconductor spintronics," Acta Phys. Slovaca **57**, 565 (2007).
[36]M. V. Fischetti, "Effect of the electron–plasmon interaction on the electron mobility in silicon," Phys. Rev. B **44**, 5527–5534 (1991).
[37]K. Ando, M. Morikawa, T. Trypiniotis, Y. Fujikawa, C. H. W. Barnes, and E. Saitoh, "Direct conversion of light-polarization information into electric voltage using photoinduced inverse spin-Hall effect in Pt/GaAs hybrid structure: Spin photodetector," J. Appl. Phys. **107**, 113902 (2010).
[38]SuperK Extreme EXW-12 (NKT photonics), providing for pulses in the nanosecond range at a 78 MHz repetition rate. In our measurements the temporal structure of the laser source can be safely neglected since the temporal average of the time-dependent spin drift–diffusion corresponds to the solution for the spin drift–diffusion equation in the steady-state, see Ref. 29.
[39]*Fundamental of Carrier Transport*, 2nd ed., edited by M. Lundstrom (Cambridge University Press, Cambridge, UK, 2000).
[40]R. J. Elliott, "Theory of the effect of spin–orbit coupling on magnetic resonance in some semiconductors," Phys. Rev. **96**, 266–279 (1954).
[41]Y. Yafet, "*g* factors and spin–lattice relaxation of conduction electrons," Solid State Phys.: Adv. Res. Appl. **14**, 1–98 (1963).
[42]M. V. Fischetti and S. E. Laux, "Monte Carlo analysis of electron transport in small semiconductor devices including band-structure and space–charge effects," Phys. Rev. B **38**, 9721–9745 (1988).
[43]Y. Song, O. Chalaev, and H. Dery, "Donor-driven spin relaxation in multivalley semiconductors," Phys. Rev. Lett. **113**, 167201 (2014).
[44]Z. G. Yu and M. E. Flatté, "Electric-field dependent spin diffusion and spin injection into semiconductors," Phys. Rev. B **66**, 201202 (2002).
[45]Z. G. Yu and M. E. Flatté, "Spin diffusion and injection in semiconductor structures: Electric field effects," Phys. Rev. B **66**, 235302 (2002).
[46]M. I. Miah, "Drift–diffusion crossover and the intrinsic spin diffusion lengths in semiconductors," J. Appl. Phys. **103**, 063718 (2008).
[47]F. Bottegoni, H.-j. Drouhin, G. Fishman, and J.-e. Wegrowe, "Probability- and spin-current operators for effective Hamiltonians," Phys. Rev. B **85**, 235313 (2012).
[48]C. Zucchetti, M. Bollani, G. Isella, M. Zani, M. Finazzi, and F. Bottegoni, "Doping dependence of the electron spin diffusion length in germanium," APL Mater. **7**, 101122 (2019).

© Author(s) 2023